



Reconstruction of a flux transfer event based on observations from five THEMIS satellites

A. T. Y. Lui,¹ D. G. Sibeck,² T. Phan,³ J. P. McFadden,³ V. Angelopoulos,⁴ and K.-H. Glassmeier⁵

Received 20 March 2008; revised 10 June 2008; accepted 16 June 2008; published 17 September 2008.

[1] We investigate a flux transfer event (FTE) observed by Time History of Events and Macroscale Interactions during Substorms (THEMIS) near the duskside magnetopause using the reconstruction technique based on solving the Grad-Shafranov equation; see review by Sonnerup et al. (2006). THEMIS D detected the FTE with the largest core magnetic field. THEMIS B and C observed deep troughs in the magnetic field associated with the FTE. THEMIS A and E sensed only slightly altered magnetic field from their surroundings. Two-dimensional reconstruction maps of magnetic field and plasma pressure are generated by combining observations from all five THEMIS satellites. These reconstructed maps show distinct differences between a magnetic island and an FTE in terms of vector potential and the derived plasma parameters. The origin of the magnetic field troughs in the crater FTEs can be traced to intrusions of the magnetosheath plasma around the structure in the reconstruction maps. Furthermore, the resulting maps show also cylindrical asymmetry in these parameters between the magnetosheath and magnetospheric sides of the FTE. This asymmetry and the different impact parameters of these satellites with respect to the FTE center together contribute to the different characteristics of the FTE signatures seen by the five THEMIS satellites.

Citation: Lui, A. T. Y., D. G. Sibeck, T. Phan, V. Angelopoulos, J. P. McFadden, and K. H. Glassmeier (2008), Reconstruction of a flux transfer event based on observations from five THEMIS satellites, *J. Geophys. Res.*, *113*, A00C01, doi:10.1029/2008JA013189.

1. Introduction

[2] NASA's most recent magnetospheric mission is Time History of Events and Macroscale Interactions during Substorms (THEMIS) [Angelopoulos, 2008; Sibeck and Angelopoulos, 2008]. The primary objective of THEMIS is to resolve the controversy concerning the substorm initiation location in the magnetotail by placing five identically instrumented satellites aligned along the tail axis to determine incontrovertibly the propagation direction of substorm disturbances in the magnetotail. Owing to a launch delay of the mission, the planned separation of the five satellites along the tail axis was postponed for nearly one year. A decision was made to place the five satellites in the "beads on a string" configuration during this coast phase. Thus, a unique opportunity arises to probe magnetospheric structures in the near-Earth space with nearby multipoint measurements.

[3] Sibeck et al. [2008] have identified a flux transfer event (FTE) near the dusk magnetopause on 20 May 2007.

During this interval, one THEMIS satellite (THEMIS D) detected an FTE with a strong core magnetic field, while another two THEMIS satellites (THEMIS B and C) detected an FTE with deep troughs in the magnetic field strength. FTEs with this signature are called crater FTEs. The two remaining THEMIS satellites (THEMIS A and E) detected only slight magnetic field strength increases. Assisted by the results of an MHD simulation, Sibeck et al. [2008] have proposed that these different signatures of FTE arise from different impact parameters with respect to the center of the FTE by the different satellites. THEMIS D had a very low impact parameter while THEMIS B and C had moderate impact parameters. THEMIS A and E had large impact parameters.

[4] Lui et al. [2008] have reconstructed the plasma parameters around the FTE detected by THEMIS D for the event reported by Sibeck et al. [2008] using the Grad-Shafranov (GS) reconstruction technique developed previously [Sonnerup and Guo, 1996; Hau and Sonnerup, 1999; Hu and Sonnerup, 2003; Hasegawa et al., 2004a, 2005; Sonnerup et al., 2006]. They have benchmarked their reconstruction code with a theoretical model as well as with actual IRM magnetopause crossing data previously investigated by Hau and Sonnerup [1999]. In their benchmark with a theoretical model, the maximum error from the comparison of six parameters between the theoretical model and the numerical results in these 2-D reconstruction maps is 6%.

¹Johns Hopkins Applied Physics Laboratory, Laurel, Maryland, USA.

²NASA Goddard Space Flight Center, Greenbelt, Maryland, USA.

³Space Sciences Laboratory, University of California, Berkeley, California, USA.

⁴IGPP, University of California, Los Angeles, California, USA.

⁵Technical University of Braunschweig, Braunschweig, Germany.

[5] For this FTE event, *Lui et al.* [2008] have verified the appropriateness of the steady state equilibrium assumption required for the GS reconstruction by performing the minimum variance analysis and the deHoffman-Teller (HT) frame transformation. The GSM coordinates of the axes for the minimum, intermediate, and maximum variances are $B_N = (-0.4522, 0.8331, -0.3186)$, $B_M = (-0.8677, -0.4936, -0.0592)$, and $B_L = (-0.2065, -0.2497, 0.9461)$, with the eigenvalues of 4.364, 177.1, and 243.1, respectively (the coordinates of B_N and B_L were inadvertently interchanged by *Lui et al.* [2008]). The MVA result indicates a well-defined B_N axis, conforming well to a 2-D structure [see also *Lui et al.*, 2008, Figure 3]. The HT velocity V_{HT} is found to be $(-91.8, 123.6, -33.6)$ km/s. The correlation coefficient between $-(V \times B)_y$ and $-(V_{HT} \times B)_y$ is 0.969, indicating the existence of a moving frame in which the structure fits well with a relatively steady state condition. The small slope for $V - V_{HT}$ versus V_a (Alfvén velocity) shows the lack of fast flows in the transformed frame, again consistent with the steady state assumption for the structure. These results show that the observed structure has properties satisfying the assumptions for the GS reconstruction.

[6] From this procedure, *Lui et al.* [2008] have extended the observed magnetic field and plasma pressure of the FTE from THEMIS D to a two-dimensional plane. In addition, current densities associated with the FTE have been deduced in this two-dimensional plane. The result indicates that the axial current density had a peak value > 40 nA/m² with significant current densities (up to ~ 25 nA/m²) on the plane perpendicular to its axis.

[7] In this paper, we extend the previous GS reconstruction based on observations from a single THEMIS satellite to encompass observations from all five THEMIS satellites. The GS reconstruction technique has been employed to analyze observations from four Cluster measurements of magnetic islands and FTEs near the magnetopause by *Hasegawa et al.* [2004a, 2005, 2006]. Here, we extend the GS reconstruction technique even further, to encompass observations from five satellites. Naturally, the complexity in producing composite reconstruction maps increases with increasing number of satellites involved and thus is not trivial. The resulting reconstruction maps provide insights on the observed FTE and the origin of the magnetic field troughs seen in crater FTEs, which have been reported and theorized previously by several researchers [e.g., *Rijnbeek et al.*, 1987; *Farrugia et al.*, 1988; *Owen et al.*, 2008; *Sibeck et al.*, 2008].

2. THEMIS Observations

[8] It is helpful to show first the locations of THEMIS satellites around the time when the FTE was detected. Figure 1 shows the projections of the THEMIS satellites on the GSM equatorial plane with the nominal locations of the bow shock and the magnetopause. Since the satellites were very close to each other, an enlarged view is included at the bottom of Figure 1, together with a schematic representation of the FTE by the shaded region. As shown in the enlarged view, during this interval, THEMIS A was furthest from the nominal dusk magnetopause (dashed curve), followed by THEMIS E, D, C, and B in decreasing distance. For this event, the observed dusk magnetopause

was further away from the Earth than the nominal position, resulting in THEMIS D being mainly within the magnetospheric boundary layer while THEMIS B and C being mainly within the magnetosphere. THEMIS A and E were mainly in the magnetosheath still. As will be shown later in Figure 4, all five satellites detected signatures or disturbances associated with the FTE almost simultaneously, but at different locations relative to the FTE center. THEMIS D passed close to the FTE center. THEMIS C and B detected the fringe of the FTE inside the magnetosphere while THEMIS A and E detected the perturbations in the magnetosheath associated with the FTE passage inside the magnetospheric boundary layer.

2.1. THEMIS D Observations

[9] The FTE observations that provide the basis for the GS reconstruction reported here are exemplified by THEMIS D and C. Figure 2 shows the plasma and magnetic field measurements [*McFadden et al.*, 2008; *Auster et al.*, 2008] from THEMIS D encompassing the FTE interval. The GSM coordinate system is used for these parameters. During this interval, the satellite crossed the magnetopause from the magnetosheath at the start of the interval to the magnetosphere at the end. The signatures of the magnetosheath region (~ 2200 – $2201:40$ UT) are a high plasma density (~ 6 cm⁻³), tailward-duskward plasma flow ($V_x \sim -150$ km/s and $V_y \sim 100$ km/s), and fluctuating southward magnetic field. Observations by the ACE satellite (not shown) indicate that the solar wind had a southward magnetic field component from ~ 1900 UT to ~ 2230 UT at 1 AU. In the magnetospheric region near the end of the interval ($\sim 2204:30$ – 2205 UT), the plasma characteristics were very different, having a low plasma density (~ 0.1 cm⁻³) and nearly stagnant ($V_x, V_y, V_z \sim 0$ km/s) with a steady northward magnetic field component ($B_z \sim 20$ nT). In between these two regions is the boundary layer ($\sim 2201:40$ – $2204:30$ UT). At ~ 2202 UT within this boundary layer interval, THEMIS D detected magnetic field characteristics quite distinct from both the magnetosheath and the magnetosphere. A prominent feature with a strong B_z component was detected for < 1 min. The two vertical dashed lines in Figure 2 mark the interval in which the structure was observed, showing the asymmetry of a lower B_z value at the start of the FTE interval than at the end. A bipolar signature can be seen in both the B_x and B_y components associated with the enhancement of the B_z component. These characteristics are commonly recognized as that of an FTE [*Russell and Elphic*, 1978].

2.2. THEMIS C Observations

[10] The plasma and magnetic field data at THEMIS C are shown in Figure 3. THEMIS C was close to THEMIS D and was further into the magnetosphere. As a result, it was mostly inside the magnetosphere observing a low plasma density, relatively stationary plasma with a high northward magnetic field component (~ 20 nT). There is one noticeable exception. At about the same time when THEMIS D detected the high core magnetic field of an FTE, THEMIS C detected a distinct feature with two depressions in the B_z component. The two vertical dashed lines in Figure 3 mark the time interval in which the structure was detected. There was an asymmetry in the B_z component, with the B_z

2007 May 20 2100 - 2300 UT

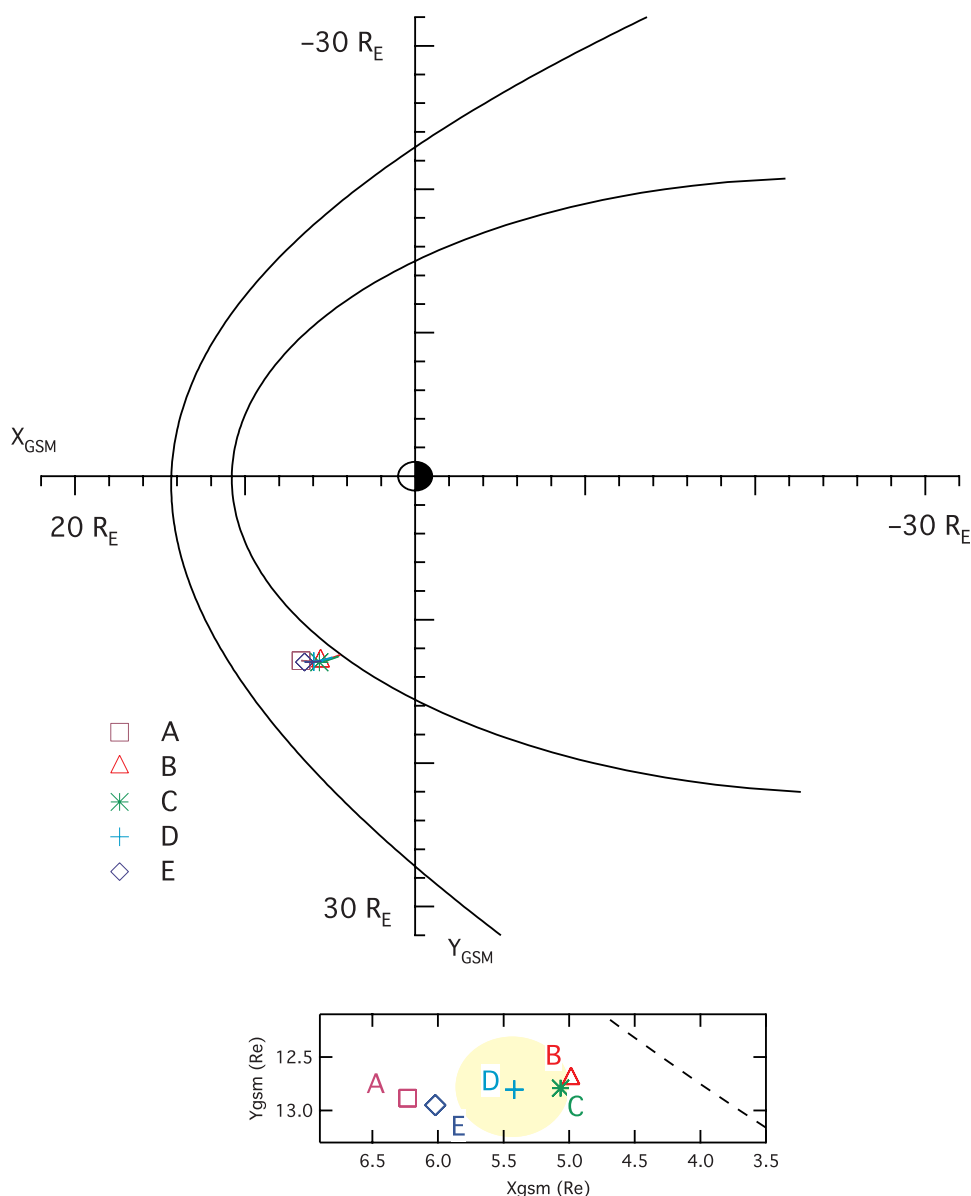


Figure 1. Projections of THEMIS satellites onto the GSM equatorial plane together with an enlarged view of the satellite locations relative to the nominal magnetopause (dashed line) and a schematic representation of the flux transfer event during its transit by the satellites.

minimum deeper near the start of the interval than near the end. A bipolar signature can be seen in both the B_x and the B_y components during this interval. These characteristics are indicative of a crater FTE. In comparison, the core magnetic field strength of the crater FTE was noticeably lower than that seen at THEMIS D. This difference in the magnetic field strength indicates that THEMIS C did not encounter the FTE as close to its center as THEMIS D. This inference is consistent with the presence of the deep minima [Sibeck *et al.*, 2008].

2.3. Observations From All THEMIS Satellites

[11] Figure 4 provides a brief overview of observations from all five THEMIS satellites during this interval. The

relative positions of these satellites at 2202 UT are also shown by the rightmost panel in the bottom row of Figure 4, in which the nominal magnetopause is given by the dashed curve. Although THEMIS A was immersed well within the magnetosheath during this interval as indicated by the fast tailward-duskward plasma flow and high number density, it observed an enhancement in the B_y component and a reduction of the V_x component at ~ 2202 UT when the FTE passed over THEMIS D. THEMIS E observations are very similar to that of THEMIS A, indicating similar effects at THEMIS E when the FTE passed over THEMIS D. There are some similarities between observations from THEMIS B and C.

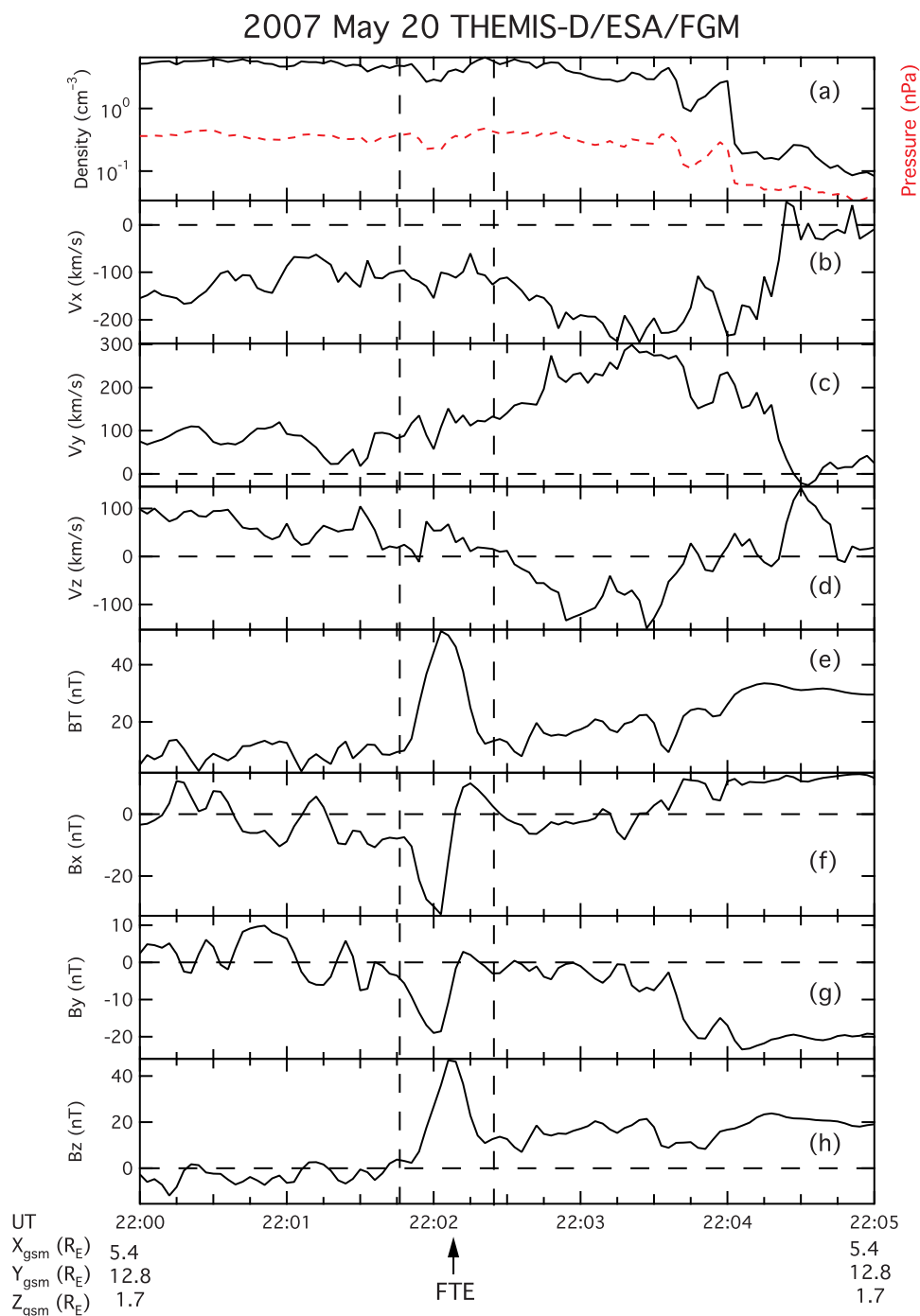


Figure 2. Plasma parameters near the dusk magnetopause measured by THEMIS D for the flux transfer event on 20 May 2007: (a) the number density is given by the solid line, and the pressure is given by the dashed line; (b–d) the three components of the plasma bulk flow; (e–h) the total magnitude and the three components of the magnetic field.

Both were mostly in the magnetosphere sampling a low density and relatively stationary plasma with a strong northward magnetic field. Both encountered significant departures from these plasma characteristics when the FTE passed over THEMIS D. There are some differences as well. THEMIS B only saw a single depression in the B_z component and a bipolar signature in the B_y component, but not in the B_x component, when the FTE passed

over THEMIS D. This indicates that THEMIS B was even further from the FTE center than THEMIS C.

3. GS Reconstruction of THEMIS Observations

3.1. Underlying Principle for Reconstruction

[12] As discussed by *Sonnerup et al.* [2006] and *Hasegawa et al.* [2004a, 2005], reconstruction of plasma configuration from observations by a single satellite and multiple satellites

2007 May 20 THEMIS-C/ESA/FGM

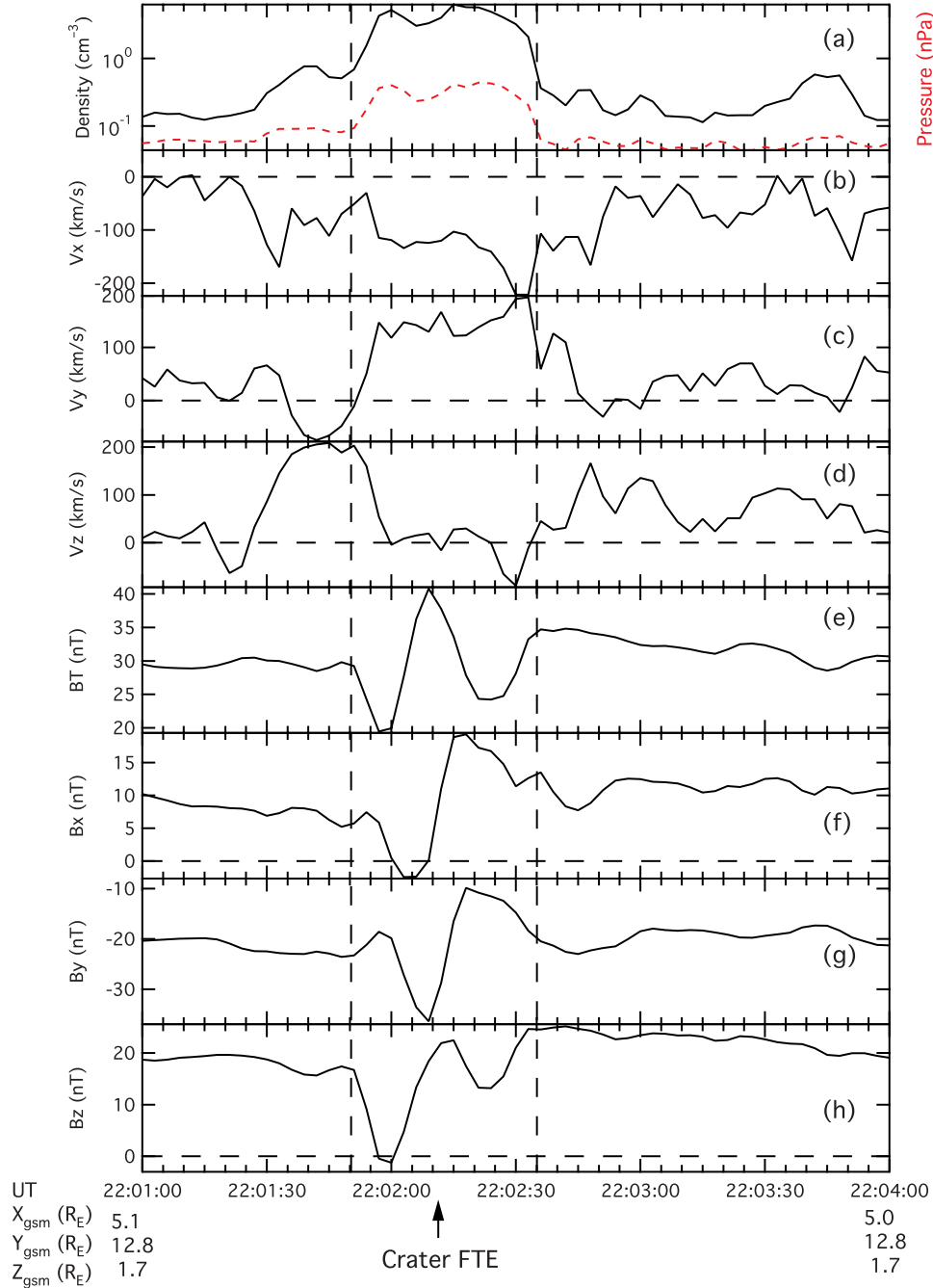


Figure 3. Plasma parameters measured by THEMIS C for the flux transfer event on 20 May 2007.

is based on solving the Grad-Shafranov (GS) equation assuming the structure is two-dimensional and is in MHD equilibrium. The GS equation is

$$\left(\frac{\partial^2}{\partial x^2} + \frac{\partial^2}{\partial y^2} \right) A = -\mu_0 \frac{dP_t(A)}{dA},$$

where the transverse pressure is given by $P_t = p + B_z^2 / 2\mu_0$. The magnetic field vector \mathbf{B} is related to the partial vector potential $A(x,y)$ and the axial magnetic field B_z by $\mathbf{B} = \nabla A(x,y) \times \hat{z} + B_z(A) \hat{z}$. The third dimension is considered as

the invariant axis, representing the direction along which the structure changes much less than the variation on the plane perpendicular to it. The approach in solving the GS equation is treating it as a spatial initial value problem. The transverse pressure and the axial magnetic field component B_z are modeled by a combination of polynomial and exponential functions of the partial vector potential $A(x,y)$.

3.2. Reconstruction Procedure

[13] *Lui et al.* [2008] have adopted the procedure documented by *Hau and Sonnerup* [1999] to reconstruct

2007 May 20 21:56-22:06 THEMIS-A,B,C,D,E

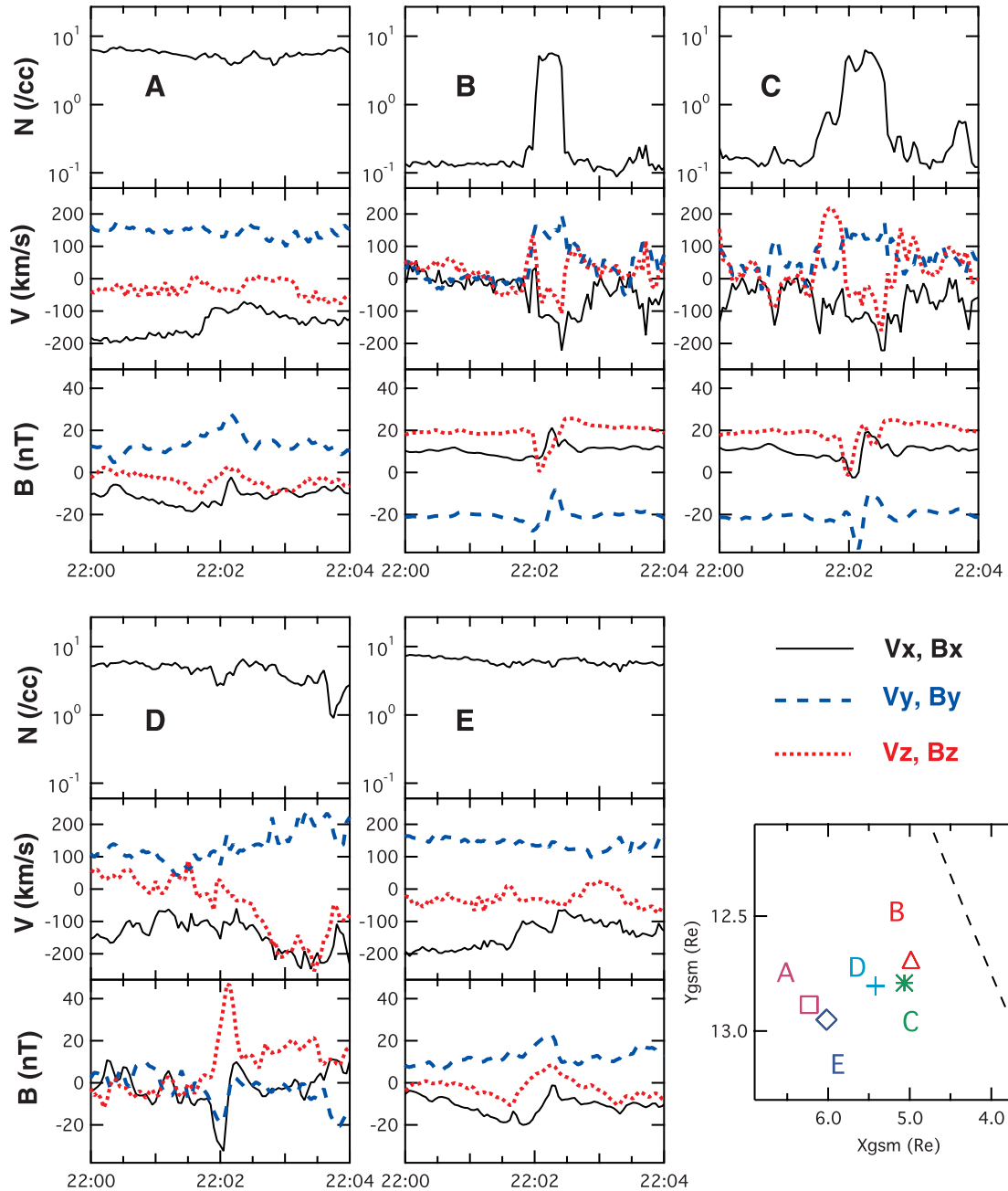


Figure 4. A brief overview of plasma parameters observed by all THEMIS satellites for the flux transfer event on 20 May 2007.

two-dimensional maps of plasma parameters based on observations from a single satellite. Our previous analysis as described in Section 1 indicates that the observed structure has properties satisfying the assumptions for GS reconstruction. As recognized by *Hu and Sonnerup* [2003], different branches of the functions for P_t and B_z may be needed to model parameters associated with the magnetosheath and with the magnetosphere. In our previous modeling effort of this FTE, these different branches are connected based on one single reconstruction, indicating more definitely than before on the basis

of the vector potential that the FTE is indeed a union of these two regions.

[14] For the composite reconstruction performed in this study, we adopt mostly the procedure documented by *Hasegawa et al.* [2004a] with some slight modifications stated below. First, since THEMIS D encountered the FTE close to its center, we adopt the coordinate system for the composite reconstruction to be that used in our previous work, following the procedure of *Hau and Sonnerup* [1999] in determining the reconstruction axes. The resulting axes for the reconstruction are $X = (0.5268, -0.7761, 0.3466)$,

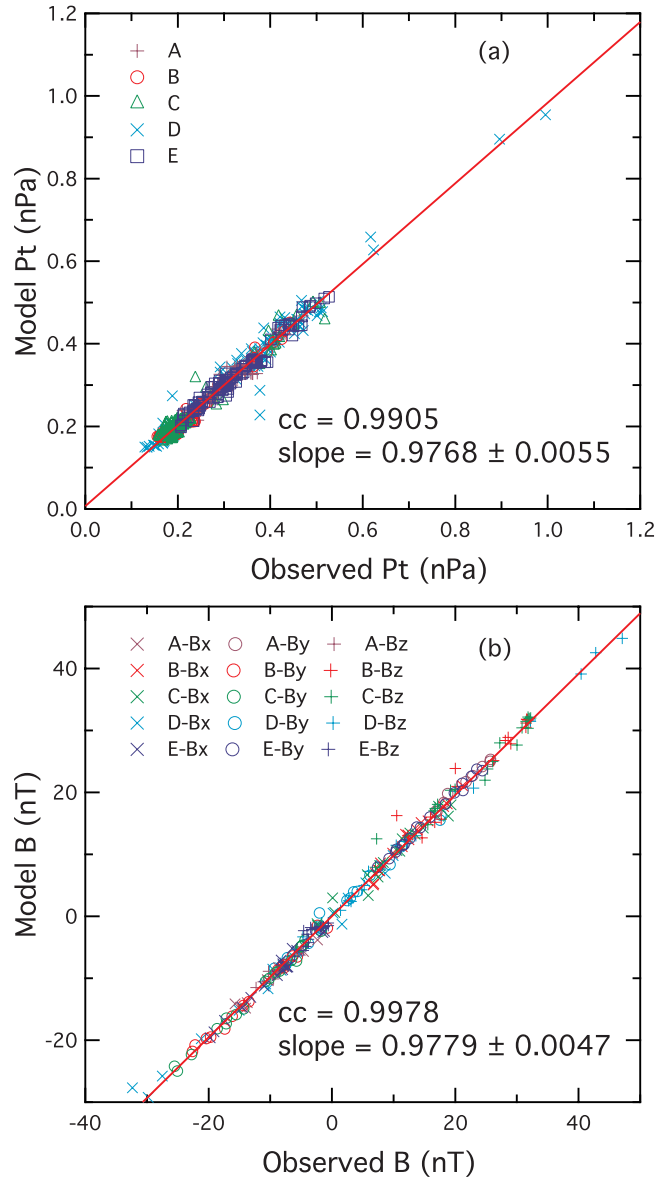


Figure 5. Comparison between the observed and modeled values for (a) the transverse pressure and (b) the axial magnetic field component.

$Y = (0.7366, 0.6203, 0.2694)$, and $Z = (-0.4241, 0.1134, 0.8985)$ in GSM coordinates. These axes were obtained through a number of rotations starting from the minimum variance axes to determine the optimal orientation of the axes for reconstruction. We shall refer to this coordinate system as the GS coordinate system. Observations from each satellite are then used individually to perform the reconstruction. The results are presented before proceeding to show the results from the composite reconstruction with observations from all five satellites. Care is taken to incorporate the relative separation distances in both the X and the Y coordinates on the GS plane at a given time. Second, since the derived partial vector potential $A(x,y)$ from each satellite satisfies the GS equation whereas any combination of these separate $A(x,y)$ does not necessarily satisfy the GS equation, we minimize the width of the transition region in producing the partial vector potential

$A(x,y)$ for the entire region by adopting a top-hat function bordered by cosine edges. More specifically, the edge function is given by

$$f(x) = 0.5 \times [1 + \cos(x/d)\pi],$$

where x is the distance from the top-hat edge and d is the width of the edge. This function allows gradual tapering of $A(x,y)$ at the transition boundary between adjacent GS solutions. This procedure is different from that of *Hasegawa et al.* [2005] who used a Gaussian function as the weight to join the partial vector potentials from different GS solutions. Third, since an arbitrary constant can be added to $A(x,y)$ without causing any change in the derived parameters of magnetic field components and plasma pressure, the continuity of $A(x,y)$ at the interfaces of two adjacent reconstruction maps is achieved by adding the average

2007 May 20 Reconstruction Map of Vector Potential

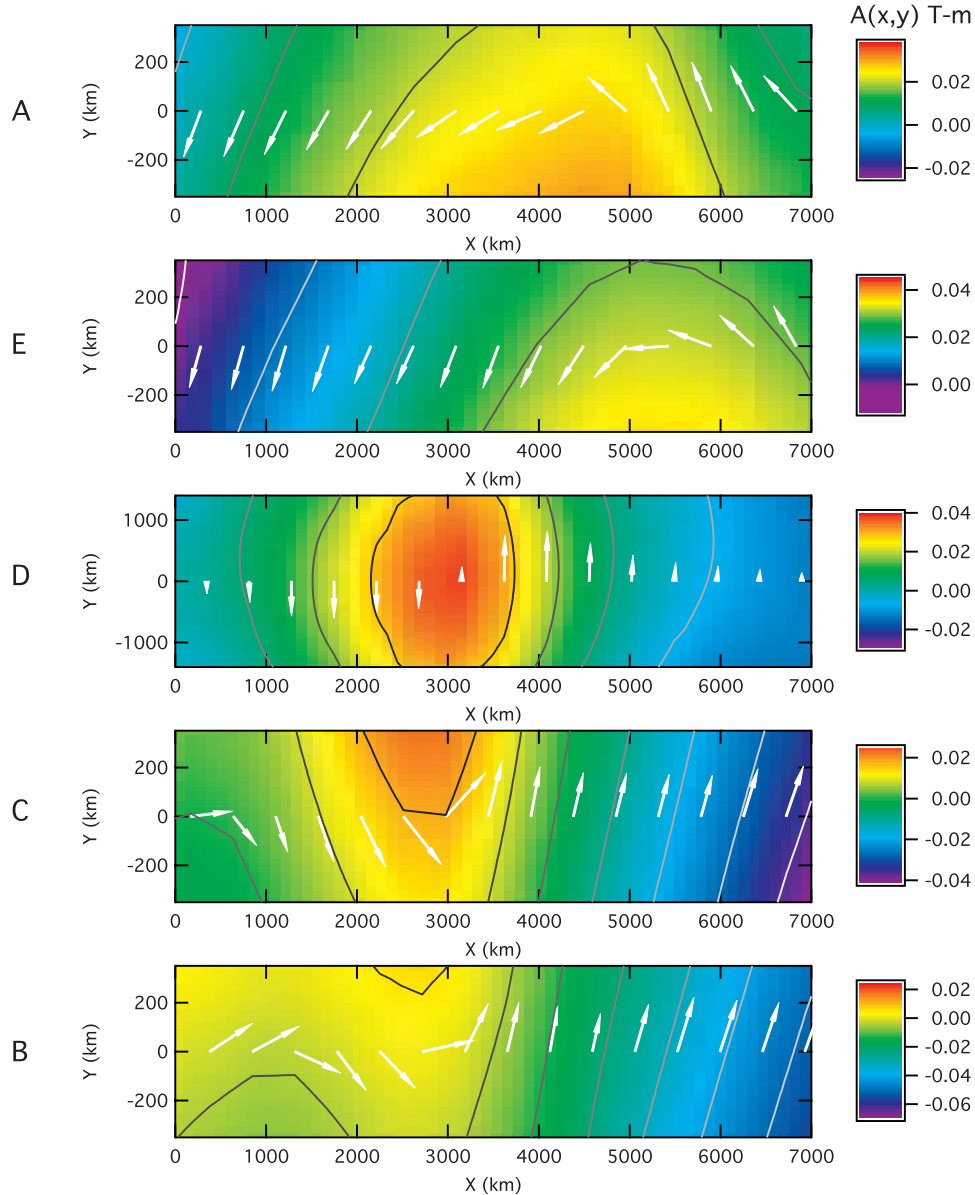


Figure 6. Two-dimensional maps of the partial vector potential for five THEMIS satellites obtained from the Grad-Shafranov (GS) reconstruction based on measurements from each individual satellite.

difference of the $A(x,y)$ from the two reconstruction maps at the relevant interface boundary.

3.3. Comparison Between Observed and Modeled Parameters

[15] The accuracy of the reconstruction results can be verified by the comparison of the observed values of P_t and the magnetic field components with the model values. Figure 5a shows the comparison between the observed and modeled P_t for all five satellites. Similarly, Figure 5b shows the comparison between observed and modeled magnetic field components for all satellites. For the P_t graph, different symbols are used for each satellite. For the magnetic field graph, different symbols are used to denote different components. The plots indicate that there are good agreements between the observed values of P_t and

the magnetic field components. For a more quantitative comparison, we have performed linear fits to these parameters. The correlation coefficients and the slopes of these fits are given in Figure 5. For the P_t parameter, the correlation coefficient and the slope are 0.9905 and 0.9768 ± 0.0055 , respectively. For the magnetic field components, the correlation coefficient and the slope are 0.9978 and 0.9779 ± 0.0047 , respectively. The values of these parameters are close to unity, indicating very good matches in general between the observed and modeled values of both P_t and the magnetic field components for the reconstruction.

3.4. Reconstruction From Individual Satellite Data

[16] The reconstruction map of $A(x,y)$ from each of five satellites is shown in Figure 6. The panels from the top to the bottom correspond to the 2-D maps from satellites with

2007 May 20 Reconstruction Maps

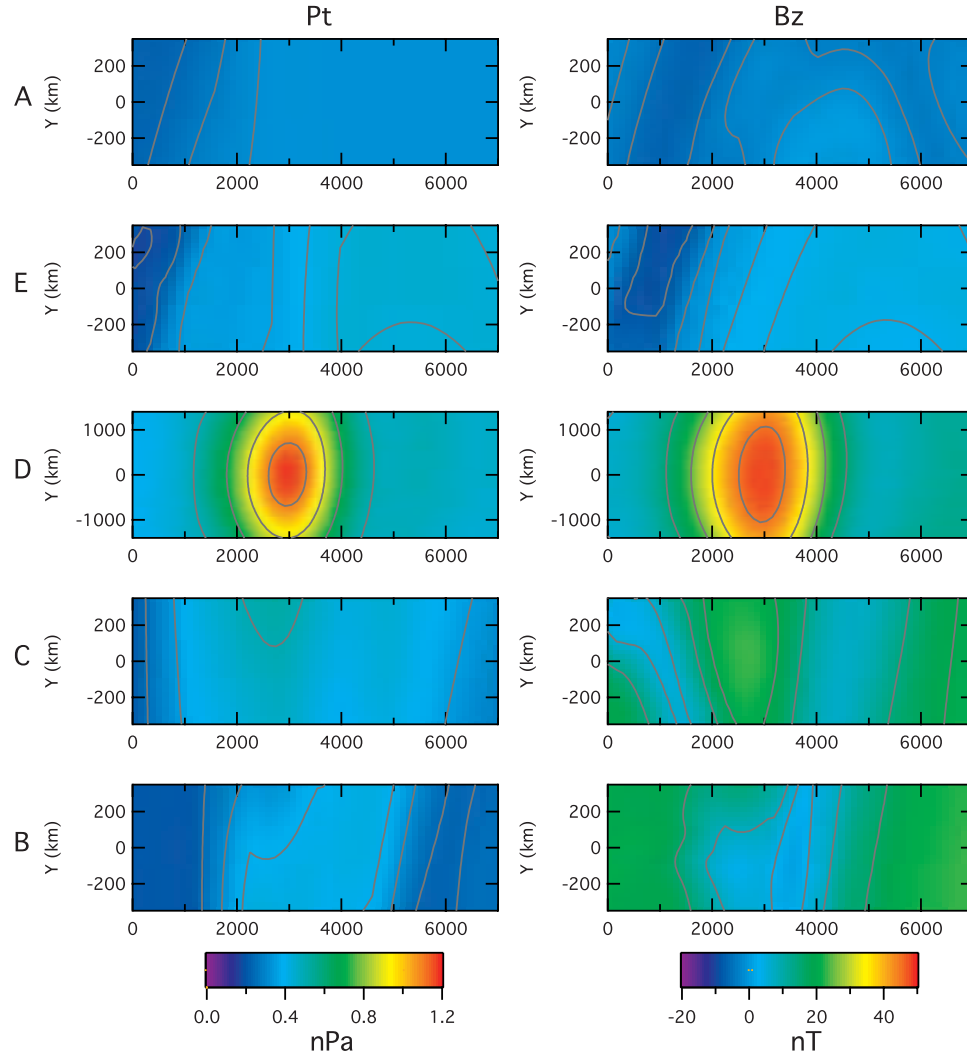


Figure 7. Two-dimensional maps of the transverse plasma pressure and the axial magnetic field component for the five THEMIS satellites reconstructed individually on the basis of measurements of each satellite.

decreasing distance from the Earth. In each panel, the observed magnetic field vectors projected on the GS XY plane along the satellite path are given by the arrows along the X axis. Transforming the satellite locations to the GS coordinate system indicates that THEMIS B and C were below THEMIS D in terms of their GS Y coordinates whereas THEMIS A and E were above THEMIS D. For orientation purposes, it should be noted that THEMIS D were in the magnetospheric boundary layer passing close to the FTE center. The nearly vertical orientation of arrows in the THEMIS D panel reinforces the result that THEMIS D indeed passed very close to the center of the FTE. The GS Y axis points away from the Earth. Therefore, during the FTE transit, THEMIS A and E were mainly in the magnetosheath while THEMIS B and C were mainly inside the magnetosphere proper. THEMIS C detected a structure appearing from the upper edge in the region centered at $X = 2700$ km. This structure corresponds to the lower edge of the FTE seen by THEMIS D, consistent with the fact that THEMIS

C was below THEMIS D. THEMIS B detected a similar structure but with less variations in the partial vector potential. These characteristics are consistent with THEMIS B being located below both THEMIS D and C so that the FTE influence is less than that of THEMIS C. THEMIS A detected a feature appearing from the lower edge in the region centered at $X = 4500$ km, which is consistent with the fact that THEMIS A was above THEMIS D on the GS XY plane. THEMIS E detected a similar feature appearing from the lower edge just like THEMIS A. Again, this is consistent with THEMIS E being above THEMIS D on the GS XY plane.

[17] The reconstruction maps of P_t (left column) and B_z (right column) for each of the five satellites are shown in Figure 7. The FTE is quite prominently seen in the reconstruction maps of P_t and B_z for THEMIS D. THEMIS C was closest to THEMIS D and detected an edge of the FTE centered around $X \sim 3000$ km. The area of enhanced values associated with the FTE edge is more obvious in the B_z

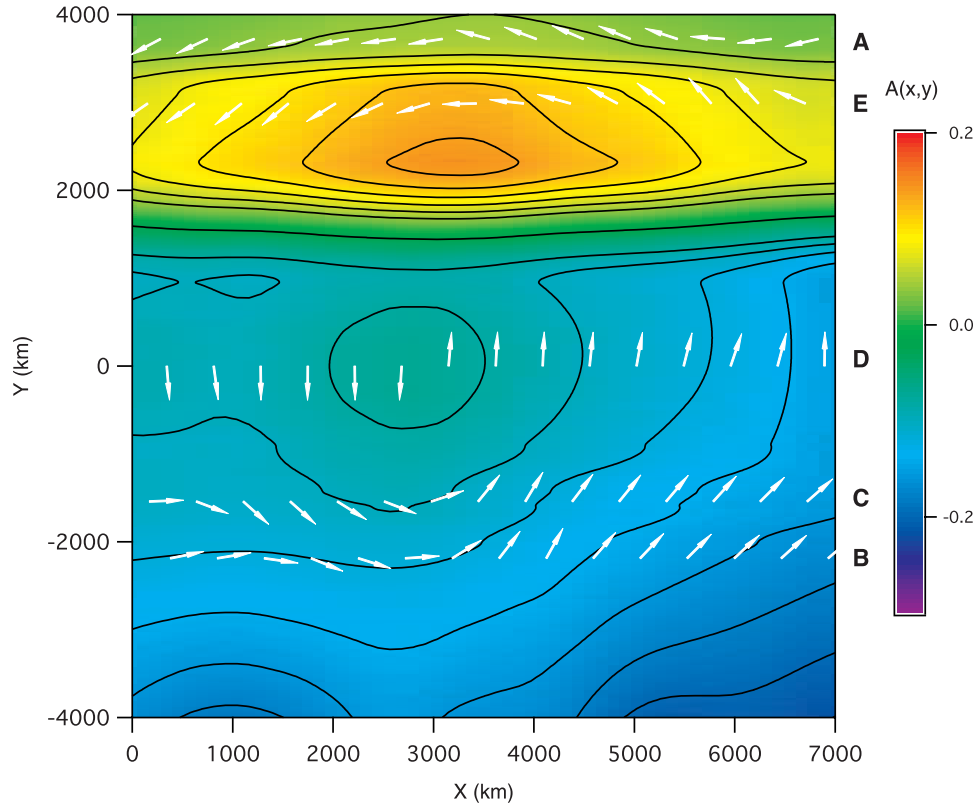
Reconstruction Map of $A(x,y)$ For THEMIS Satellites A-E

Figure 8. Composite reconstruction map of the partial magnetic vector potential with the overlay of the observed magnetic field vectors projected on the GS XY plane from each THEMIS satellite.

panel and less so in the P_t panel. There were very little indications of the FTE effect from the reconstruction maps of the other three THEMIS satellites.

3.5. Composite Reconstruction of Data From All Five THEMIS Satellites

[18] The results of the composite reconstruction are given in Figures 8 and 9. Since THEMIS D traversed the FTE closest to its center, we adopt the X axis of the composite reconstruction map to be along the THEMIS D path. In the GS coordinate system, THEMIS B has the lowest Y coordinate and thus its map is used as the starting point of the composite reconstruction. The relative displacements of these five satellites with respect to each other in the X direction are taken into account in this composite reconstruction so that the parameter maps from different satellites can be matched properly. The composite partial vector potential is shown in Figure 8 with the overlaid of the magnetic field vectors seen by the five satellites projected on the GS XY plane. The identifications of the THEMIS satellites are indicated on the right hand side of the graph.

[19] The reconstruction map in Figure 8 shows well the FTE along the THEMIS D path (X axis). It also shows THEMIS D crossing very close to the center of the FTE structure as mentioned before. Just above the FTE are some nearly parallel isocontours which probably mark the transition from the magnetospheric boundary layer to the mag-

netosheath proper. Above these isocontours is a magnetic island structure that lies slightly below the paths of THEMIS A and E. Below the FTE, the isocontours are bent downward owing to the existence of the FTE, representing the distortion of the magnetospheric boundary.

[20] Reconstruction maps of transverse and plasma pressures, axial magnetic field, and axial current density are shown in Figure 9. The axial current density J_z is computed by the Ampere's law with the assumption of a negligible contribution from the displacement current, i.e., $J_z = (\partial B_y / \partial x - \partial B_x / \partial y) / \mu_0$. The horizontal straight lines in these maps indicate paths of the five satellites in the GS XY plane. Labels of each satellite are given on the right hand side of the reconstruction map for the transverse pressure. The FTE shows up more prominently in these construction maps than the magnetic island in the magnetosheath. On the other hand, the magnetic island seen prominently in the partial vector potential map does not have a similar prominence in these other maps. This result suggests a clear distinction between a magnetic island in the magnetosheath and an FTE embedded within the boundary layer. Another noticeable feature is that the parameters shown in these maps show significant differences between the regions above and below the FTE. This difference, evident in the B_z reconstruction map, is mostly due to the intrusion of plasma from the magnetosheath region on the right hand side of the map above the FTE at $(X, Y) = (7000, 2000)$ km to the

Reconstruction Maps For THEMIS Satellites A-E

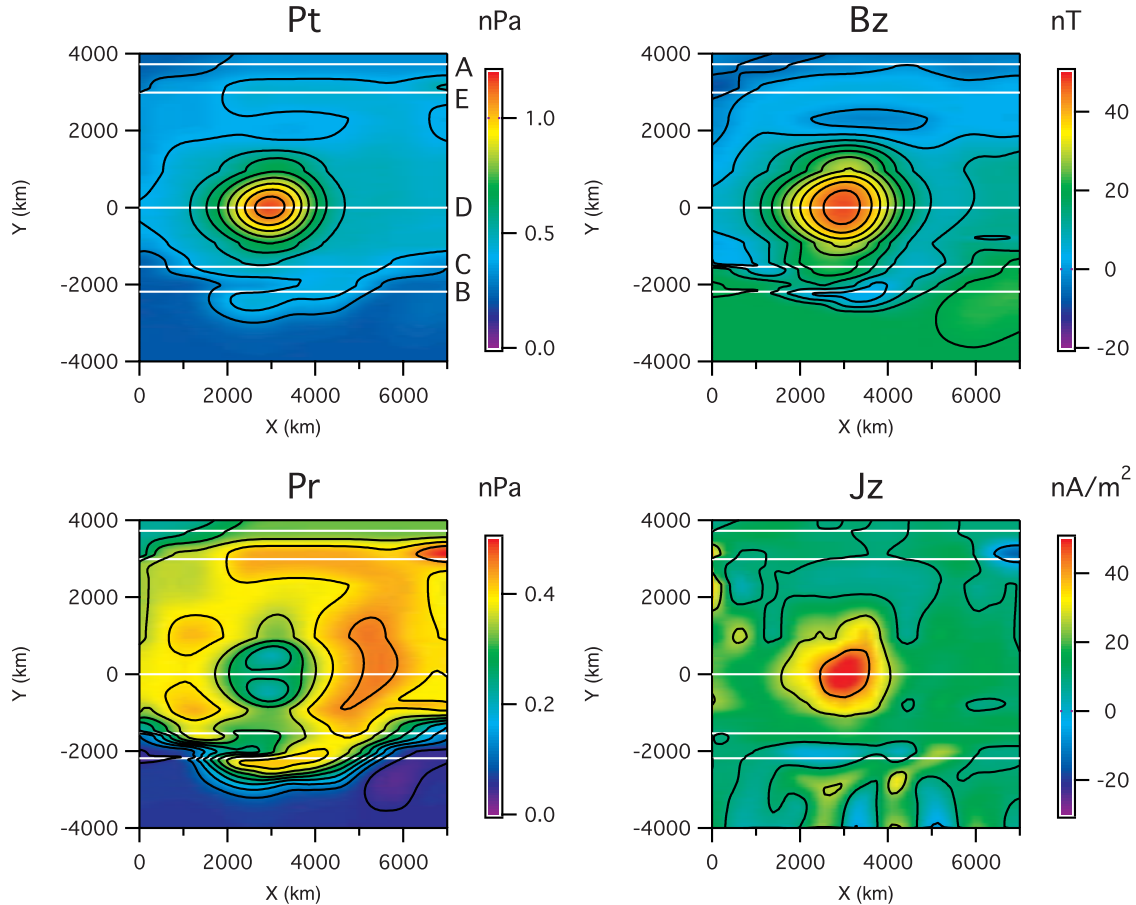


Figure 9. Composite reconstruction maps of the transverse pressure, the axial magnetic field component, the plasma pressure, and the axial current density based on combined measurements from all five THEMIS satellites.

magnetospheric region below the FTE at $(X, Y) = (3000, -2000)$ km.

4. Summary and Discussion

[21] We have developed independently the technique to perform the Grad-Shafranov reconstruction from multiple satellite observations following similar procedures documented previously with some slight modifications in the reconstruction of the composite maps [Sonnerup and Guo, 1996; Hau and Sonnerup, 1999; Hasegawa *et al.*, 2004a, 2005; Sonnerup *et al.*, 2006, and references therein]. We apply the technique to the FTE detected by the THEMIS satellites near the dusk magnetopause on May 20 2007 [Sibeck *et al.*, 2008]. Significant differences exist in the observed plasma parameters from these five THEMIS satellites.

[22] Two-dimensional maps of plasma parameters are first reconstructed individually for each THEMIS satellite. These results are presented to show how the FTE influence is seen in the reconstruction maps from each satellite located at different distances from the center of the FTE. This is followed by combining measurements from all five THEMIS satellites to produce two-dimensional composite re-

construction maps of plasma parameters of the FTE and its surroundings. From the composite maps, the total magnetic flux and the total current content within the FTE are found to be 0.30 MWeber and 0.22 MA, respectively. Hasegawa *et al.* [2006] have examined five FTEs for the total magnetic flux and current contained within these FTEs. The results show that the total magnetic flux ranges from 1.05 to 3.59 MWeber in magnitude and the total current ranges from 0.39 to 0.70 MA in magnitude. The FTE examined in this report has smaller values in these parameters because the size of this FTE is only ~ 4000 km whereas those examined by Hasegawa *et al.* [2006] have sizes ranging from ~ 7000 to 20000 km.

[23] The composite results show some interesting features that have not been noted before. First, a magnetic island in the magnetosheath region appears quite prominently in the partial vector potential $A(x,y)$ map but is not conspicuous in the maps of the B_z component, the transverse pressure P_t , the plasma pressure P_r , and the axial current density J_z . On the other hand, the FTE is less conspicuous in the $A(x,y)$ map but stands out prominently in the maps of other parameters. This is due to the different branches of the functions for the magnetosheath and the magnetosphere in modeling the P_t and the B_z component. The magnetic island

is on the magnetosheath branch where the P_t and the B_z component do not change significantly over a large range of $A(x,y)$. On the other hand, the FTE is on the magnetospheric branch where the P_t and the B_z component change significantly for the values of $A(x,y)$ associated with the FTE. Second, from the $A(x,y)$ and B_z maps, the magnetic field troughs bounding the FTE are due to intrusions of the weak B_z region near the magnetosheath. This weak B_z region only appears prominently in the strong background magnetic field of the magnetosphere (in THEMIS B and C observations) but not in the weak background magnetic field of the magnetospheric boundary layer (in THEMIS D observations). Third, the FTE exhibits asymmetric structures in the boundary layer between the magnetosphere proper and the magnetosheath proper, especially in the B_z and P_t maps. This asymmetry together with the differences arising from the different impact parameters of these satellites may collectively account for the different signatures seen by these five THEMIS satellites during the FTE encounter.

[24] One may wonder whether there is any implication in the simultaneous occurrence of a magnetic island in the magnetosheath and an FTE in the magnetospheric boundary layer. One plausible implication relates to the evolution of an FTE. When an interplanetary magnetic field (IMF) line reconnects with a closed geomagnetic field line, two open magnetic field lines in opposite hemispheres are formed, giving rise to FTEs seen in both hemispheres. Subsequently, the two open field lines reconnect with each other again in the equatorial plane to form a closed magnetic field line and a magnetic field line disconnected from the Earth. The simultaneous presence of an FTE inside the magnetospheric boundary layer and a magnetic island in the magnetosheath is what is expected for the second stage of reconnection. One side of the magnetic field lines in the FTE evolves by another reconnection process, instigated perhaps by the Kelvin-Helmholtz instability [Nykyri and Otto, 2001; Hasegawa et al., 2004b; Nykyri et al., 2006], to become a feature with closed magnetic field lines in the magnetospheric boundary layer. The other side of the magnetic field lines in the FTE evolves by the same reconnection process to become the magnetic island in the magnetosheath, separating it from the part in the magnetospheric boundary layer. This evolution is similar to that of Dungey's proposal except that the open magnetic field lines formed by the dayside reconnection for this FTE detected near the dusk equatorial magnetopause are carried along the low-latitude boundary layer instead of over the polar cap.

[25] **Acknowledgments.** This work was supported by NASA grant NAS5-02099 to University of California, Berkeley, and by the NSF grant ATM-0630912 and NASA grant NNX07AU74G to The Johns Hopkins University Applied Physics Laboratory. The work of K.H.G. was financially supported by the German Ministerium für Wirtschaft und Technologie and the German Zentrum für Luft- und Raumfahrt under grant 50QP0402.

[26] Zuyin Pu thanks Malcolm Dunlop and another reviewer for their assistance in evaluating this paper.

References

- Angelopoulos, V. (2008), The THEMIS mission, *Space Sci. Rev.*, doi:10.1007/s11214-008-9336-1, in press.
- Auster, U., et al. (2008), The THEMIS fluxgate magnetometer, *Space Sci. Rev.*, doi:10.1007/s11214-008-9365-9, in press.
- Farrugia, C. J., et al. (1988), A multi-instrument study of flux transfer event structure, *J. Geophys. Res.*, *93*(A12), 14,465–14,477, doi:10.1029/JA093iA12p14465.
- Hasegawa, H., et al. (2004a), Reconstruction of two-dimensional magnetopause structures from Cluster observations: Verification of method, *Ann. Geophys.*, *22*, 1251–1266.
- Hasegawa, H., et al. (2004b), Transport of solar wind into Earth's magnetosphere through rolled-up Kelvin-Helmholtz vortices, *Nature*, *430*, 755–757, doi:10.1038/nature02799.
- Hasegawa, H., et al. (2005), Optimal reconstruction of magnetopause structures from Cluster data, *Ann. Geophys.*, *23*, 973–982.
- Hasegawa, H., et al. (2006), The structure of flux transfer events recovered from Cluster data, *Ann. Geophys.*, *24*, 603–618.
- Hau, L.-N., and B. U. Ö. Sonnerup (1999), Two-dimensional coherent structures in the magnetopause: Recovery of static equilibria from single-spacecraft data, *J. Geophys. Res.*, *104*, 6899–6917, doi:10.1029/1999JA900002.
- Hu, Q., and B. U. Ö. Sonnerup (2003), Reconstruction of two-dimensional structures in the magnetopause: Method improvements, *J. Geophys. Res.*, *108*(A1), 1011, doi:10.1029/2002JA009323.
- Lui, A. T. Y., et al. (2008), Reconstruction of a magnetic flux rope from THEMIS observations, *Geophys. Res. Lett.*, *35*, L17S05, doi:10.1029/2007GL032933.
- McFadden, J. P., et al. (2008), The THEMIS ESA plasma instrument and in-flight calibration, *Space Sci. Rev.*, in press.
- Nykyri, K., and A. Otto (2001), Plasma transport at the magnetospheric boundary due to reconnection in Kelvin-Helmholtz vortices, *Geophys. Res. Lett.*, *28*, 3565–3568, doi:10.1029/2001GL013239.
- Nykyri, K., et al. (2006), Cluster observations of reconnection due to the Kelvin-Helmholtz instability at the dawnside magnetospheric flank, *Ann. Geophys.*, *24*, 2619–2643.
- Owen, C. J., et al. (2008), Cluster observations of “crater” flux transfer events at the dayside high-latitude magnetopause, *J. Geophys. Res.*, *113*, A07S04, doi:10.1029/2007JA012701.
- Rijnbeek, R. P., et al. (1987), A magnetic boundary signature within flux transfer events, *Planet. Space Sci.*, *35*, 871–878, doi:10.1016/0032-0633(87)90065-1.
- Russell, C. T., and R. C. Elphic (1978), Initial ISEE magnetometer results: Magnetopause observations, *Space Sci. Rev.*, *22*, 681–715, doi:10.1007/BF00212619.
- Sibeck, D. G., and V. Angelopoulos (2008), THEMIS science objectives and mission phases, *Space Sci. Rev.*, doi:10.1007/s11214-008-9393-5, in press.
- Sibeck, D. G., et al. (2008), Crater FTEs: Simulation results and THEMIS observations, *Geophys. Res. Lett.*, *35*, L17S06, doi:10.1029/2008GL033568.
- Sonnerup, B. U. Ö., and M. Guo (1996), Magnetopause transects, *Geophys. Res. Lett.*, *23*, 3679–3682, doi:10.1029/96GL03573.
- Sonnerup, B. U. Ö., et al. (2006), Grad-Shafranov reconstruction: An overview, *J. Geophys. Res.*, *111*, A09204, doi:10.1029/2006JA011717.
- V. Angelopoulos, IGPP, University of California, Los Angeles, CA 90095, USA.
- K.-H. Glassmeier, Technical University of Braunschweig, Mendelssohnstrasse 3, D-38106 Braunschweig, Germany.
- A. T. Y. Lui, Johns Hopkins Applied Physics Laboratory, 11100 Johns Hopkins Road, Laurel, MD 20723-6099, USA. (tony.lui@jhuapl.edu)
- J. P. McFadden and T. Phan, Space Sciences Laboratory, University of California, 7 Gauss Way, Berkeley, CA 94720, USA.
- D. G. Sibeck, NASA Goddard Space Flight Center, 8800 Greenbelt Road, Greenbelt, MD 20771, USA.